Student ID: 3032206W

Insights into Amphotericin B resistance of Leishmania mexicana from polyomic data.

Introduction

Leishmaniasis

Leishmaniases is a group of diseases caused by the protozoan parasites of the genus Leishmania, that is present on all continents and affects approximately 700 000 – 1 million people annually (WHO, 2023). Leishmania is transmitted by sandflies feeding on mammalian blood. Noteworthy, Leishmania adopts morphologically different life forms – amastigote in the sandfly and promastigote in the host. There are at least 21 species of Leishmania affecting humans. Although the research into Leishmania remains limited, much can be extrapolated from findings in the closely related genus Trypanosoma and biochemically similar fungi. The knowledge can be similarly shared for all Leishmania species while remembering about potential differences that are still to be explored (Peacock, 2007)

Leishmaniasis are divided based on their presentations and the species of Leishmania, with visceral leishmaniasis being the most severe and fatal if left untreated. Effective chemotherapy against leishmaniasis exists; however, they are not without limitations. All of them cause a number of side effects, including renal toxicity in case of amphotericin B. The first line of treatment has long been antimonials, but a rising number of resistance cases shifted the focus onto alternatives: amphotericin B (ampB), pentamidine and miltefosine (Uliana, 2018). Although their effectiveness has been validated clinically, their mode of action has long been elusive.

AmpB usage and resistance

AmpB is an attractive drug due to its subsided cost for low- and middle-income countries (Gaffi, 2018), high effectiveness and the blood-brain barrier permeability. It's assumed mode of action is binding to sterols in the parasite membrane, specifically to cholesterol and ergosterol (Kumari et al., 2022). The attachment causes the pores to form in the membrane, through which the cations infiltrate the cell and eventually lead to cell death (Mesa-Arango et al., 2012). An alternative sterol sponge model and surface absorption model stipulate that AmpB might aggregate on the surface of the membrane, leading to the change in membrane integrity (Anderson et al, 2014).

Although rare, the cases of AmpB resistance appear clinically and are expected to rise in the future (Srivastava et al, 2011). In comparison to the long-effective pentamidine, AmpB has a longer mode of action, which might predispose it to developing resistance, as the cells have more time to adjust (Purkait et al, 2012; Graf, 2013).

Previous findings

Sterol 14α-demethylase, CYP51, is present in all biological kingdoms, sharing a high genetic conservation across closely related species (Lepesheva et al, 2006). It plays a crucial enzymatic role in sterol biosynthesis, performing the oxidative removal of methyl groups from sterol precursors (Zhang et al, 2019), such as lanosterol or obtusifoliol. The reaction results in ergosterol, which is a membrane component providing fluidity. CYP51 performs the conversion in three steps of a high special sensitivity (Zhang et al, 2019). The binding pocket of the enzyme and its blockage by azoles in was described previously in *Leishmania infantum* by Hargrove (2011). The investigation of Mwenechanya and collegues (2017) showed that AmpB resistant Leishmania infantum correlates with the absence of ergosterol, and the response is regained with its supplementation in culture.

Goal of the study

In the light of previous chemotherapies, the development of ampB resistance appears inevitable. Therefore, we employ the polyomics approach to validate previous findings of Mwenechanya and collegues (2017), who investigated the mode of action of ampB-resistant strain of *Leishmania mexicana*. The aim of the study is to provide additional insight into the drug's mode of action that might underlie counteracting the ampB resistance in the affected population.

Materials and Methods

Genomics

Culture of AmpB resistant cell lines

Amphotericin B resistant *Leishmania Mexicana* promastigote cell line was obtained with phenotypic screening for cells resistant to the drug, as described by Mwenechanya and collegues (2017). The initial concentration of the drug was 0.0135 µM AmpB (Sigma-Aldrich), whereas the maximum tolerated concentration equalled 0.27 µM. Notably, the authors note that the AmpB-resistant cells had a slower growth rate while they underwent a concentration change and showed a reduced cell body length when compared to the whild type (WT). The cells' response to other drugs was examined, revealing cross resistance to potassium antimony tartrate (PAT), miltefosine and ketoconazole. Finally, the AmpB-resistant cells were more sensitive to oxidative stress induced by methylene blue or glucose oxidase.

Genomic analysis

Genomes from both sample groups were sequenced with paired-end Illumina GAIIx next generation DNA sequencing platform and are available at the European Nucleotide Archive (ENA, project number PRJEB10872; Mwenechanya et al, 2017). Together with *Leishmania Mexicana* MHOM/GT/2001/U1103 reference genome with its annotation file (.gff), they constituted input files for the genome analysis. The analysis was performed in bash using tools named in ***Table 1***.

Table 1. Extracting SNPs unique for the AmpB-resistant cells from genome sequencing of both experimental groups. The quality of the initial sequencing files was assessed with ***FastQC*** and trimmed with ***Trim-galore*** to retain sequences without adapters and 3' ends falling below Phred quality score of 20. The reference genome of Leishmania Mexicana MHOM/GT/2001/U1103 was indexed with ***Bowtie2***. The same software was used to produce alignment of the reading per group against the reference. The results were converted, sorted, indexed and annotated with respective experimental group names with ***Samtools*** and ***bamaddrg***. The alignments are mapped on the reference genome (***Freebayes***) and the alignment coverage tracks are created (***bamCoverage***) per sample. The VCF file is again filtered based on the quality of the SNP (***vcfFilter***), and variants are split into two files based on their experimental group (***BcfTools***). Finally, the SNPs unique for the AmpB-resistant cell line (***SnpEff***) that result in the non-synonymous change of the amino acid of medium/high impact (***SnpSift***) are isolated and extracted into a tab-deliminated file (***SnpSift extractfields***).

Process	Tool	Version	Options	Reference	Explanation	Output
Quality check	**fastqc**	0.12.0	-o	Andrews S., 2010.	Examining the quality of sequencing, especially the needs. Deciding on the parameters for trimming.	Quality report in html per sequence read file
Trimming	**Trim-galore**	0.6.5	-q –phred64 –length –o –paired	Krueger, 2012	Trimming the reads based on adapter presence and read quality.	Trimmed reads
Indexing of reference genome	**Bowtie2-build**	2.5.4	-	Langmead & Salzberg, 2012; Langmead et al, 2019	Creates a Bowtie index files from the reference genome in FASTA.	Bowtie index files for the reference sequence.
Alignment	**Bowtie2**	2.5.4	--phred64 –x –S		Aligning the sequence reads to the Bowtie index.	Alignment file in .sam format
Conversion of SAM to BAM	**Samtools view**	1.21	-b	Danecek et al, 2021	Converting the .sam file to the .bam file.	Alignment file in .bam format
Sorting	**Samtools sort**		-o		Ordering the aligned reads and removing duplicates.	Sorted alignment in .bam file
Indexing	**Samtools index**		-b -o		Indexing the positions of the aligned reads.	Indexed alignment in .bai format
Annotating groups for SNP calling	**bamaddrg**	-	-b -s	Garrison, 2020	Adding experimental group names to the alignment files.	Alignment files matched with experimental groups.
SNP calling	**Freebayes**	1.3.9	-f –vcf –p --stdin	Garrison & Marth, 2012	Locates the SNPs by comparing sequences aligned to a target on the reference genome.	VCF file detailing the differential genomic features for both groups
Creating bedgraphs	**bamCoverage (deepTools)**	3.5.6	-b –o –of	Ramírez et al, 2016	Calculating the coverage of alignment over the whole reference genome.	Bedgraph/bigwig files with alignment coverage tracks
Filtering SNPs	**vcfFilter**	1.0.13	-f	Garrison et al, 2022	Filtering SNPs based on quality and the number of alleles.	VCF file with SNPs with their quality score over 20
Extracting the SNPs unique for AmpB	**Bcftools isec, Bcftools view**	1.21	isec –p view –s –c –Oz –o index -o	Danecek et al, 2021	Separating SNPs based on the samples group and isolating the SNPs detected only in the AmpB resistant sample.	VCF files with all SNPs in the sample group. VCF files with SNPs unique for a specific group.
Creating the SNP database	**SnpEff build**	5.2f	-c -gff3 -noCheckCds -noCheckProtein -v	Cingolani et al, 2012a	Creating a SnpEff database for the reference species Leishmania Mexicana.	Binary SnpEff database for the reference species.
Annotating SNPs	**SnpEff**	5.2f	-c	Cingolani et al, 2012a	Annotating the SNPs with their genomic location and predicted downstream effect.	VCF file with SNPs unique for the AmpB-resistant group with their predicted effects.
Extracting non-synonymous variants	**SnpSift extractfields**	5.2f	-	Cingolani et al, 2012b	Focusing on the SNPs that result in the change in the protein and are of moderate-high impact.	Tab-delimited file with desired SNPs.

The reads was assessed with FastQC. Subsequently, they were deprived of adapters and 3' ends falling below Phred quality score of 20 using Trim-Galore. Processed reads were matched to the reference genome with Bowtie2 using local alignment, then post-processed with Samtools, bamaddrg. BamCoverage to generate continuous alignment coverage tracks. Simultaneously, the SNP calling was performed with freebayes. At this point, the genome alignment, SNPs and coverage were examined in the IGV software as described by Robinson and collegues (2017) and shown in ***Figure 1***. The ploidy of chromosomes was estimated based on the genome coverage normalised to the median of diploid chromosmes: 23, 24, 25 and 26. Finally, VcfFilter, BcfTools, SnpEff and SnpSift were employed consequitively to extract SNPs unique for the AmpR cell line that result in a change in protein of a moderate/high effect.

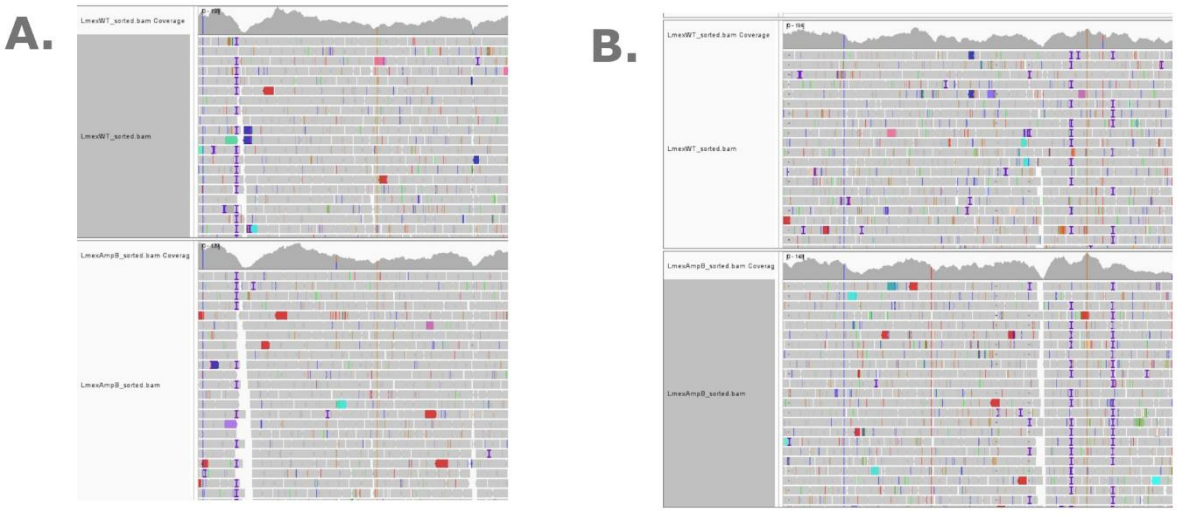

Figure 1. Visual assessment in the IGV software of the SNPs in the WT (track above) and AmpB-resistant (track below) *Leishmania Mexicana*. Presented reads were acquired with Illumina paired-reads sequencing and aligned against the reference genome MHOM/GT/2001/U1103. **A low-confidence SNP (A.**, SNP ID: LmxM.08_29.2020) shows a presence across a smaller proportion of reads, with many mutations occurring in this section of the aligned reads. It might also be accompanied by low depth of coverage or occur at the 3' of the read, where the quality decreases. In contrast, a **high-confidence SNP (B.**, SNP ID: LmxM.11.1100) has low variance in the aligned position across many reads with a clear presence or a lack thereof in contrasted samples.

Metabolomics

Mass spectrometry

The metabolome was collected with an Orbitrap Exactive Mass Spectrometer and a Sequant ZIC-HILIC column. It was further pre-processed with PMP (XCMS and MZMatch) using the RSD filter of 0.5, noise filter of 0.8, minimum detection of 3 and minimum intensity of 5000. Because of shared mass and charge, many peaks can correspond to many molecules – they cannot be initially annotated as different molecules simultaneously, causing multiplicated data. The requirement for the metabolite identification from the peak is matching an authentic standard and m/z, otherwise it is annotated based on the probable match and may not constitute a true match with a compound.

Metabolomics analysis software

The metabolomics results provided were browsed and visualised in PiMP (Gloaguen, 2017). Additional statistical analysis was performed on the Metaboanalyst server (Pang et al, 2024). Here, all missing values were replaced by k-nearest neighbors algorithm. The filters for the repeated processing were: relative standard deviation of 50% for reliability, 40% of the interquantile range for variance (expected high repeatability for the drug resistance) and no abundance filter. Data was not normalised, but log-transformed.

Proteomics

Protein structure visualisation

The investigated protein structure of Leishmania infantum sterol 14-alpha demethylase (CYP51, PDB ID 3L4D) is sourced from the investigation of Hargrove and collegues (2011) and constitutes a close homologue. The accessed complex binds with fluconazole instead of AmpB. The similarity between its sequence and *L. Mexicana* was confirmed with MView (Brown et al, 1998). Then, the subcellular localisation of the proteins was predicted with DeepLoc-2.1 (Ødum et al, 2024), whose algorithm is based on described subcellular localisations of other proteins. Although it also detects the sorting signals, this was additionally checked with SignalP-6.0 (Teufel et al, 2022). All protein structures were visualised with PyMOL.

Structure prediction software

The atomic resolution model of *L.mexicana* CYP51 N176I mutant (Mwenechanya et al, 2017) was generated with D-I-Tasser (Zheng et al, 2025) using default settings. Obtusifoliol (4α,14α-dimethyl-5α-ergosta-8,24(28)-dien-3-beta-ol; PubChem CID: 65252) was used as an alternative substrate to 14α-dimethyl-5α-ergosta-8,24(28)-dien-3-beta-ol for CYP51, and then docked to the predicted structure of the WT CYP51 (AlphaFold identifier: AF-C7FGL3-F1; Jumper, 2021) and N176I CYP51 mutant with SwissDock and its algorithm Attracting Cavities 2.0 (Röhrig, 2023) . The Gibbs free energy (ΔG) of the output docking poses were assessed in Chimera 1.18 (Petersen et al, 2004). Finally, the folding of the WT and the mutant with or without the ligand bound in time was predicted with UNRES coarsed-grained model simulations (Ślusarz et al., 2025) using the default settings and aforementioned proteins-peptide complexes.

Genomics: proteins of interest in the case of AmpB resistance

Sequence pre-processing & alignment

More sequences were collected for the WT than the ampB-R samples (***Figure 2A***). From the total of 2.2 and 2.6 Gpb, for both ampB-R pairs and both WT, respectively, 11.2-17% were discarded based on quality below Phred score of 20 at the 3' end (***Figure 2B***). Around every fourth read was also contaminated with adapters. The quality per base and per tile improved significantly after trimming, as exemplified in ***Figure 2C***. A total of 82.75% and 79.64% of reads aligned concordantly for ampB-resistant and WT samples, respectively. Out of those, a respective 9.48% and 7.50% aligned concordantly more than once.

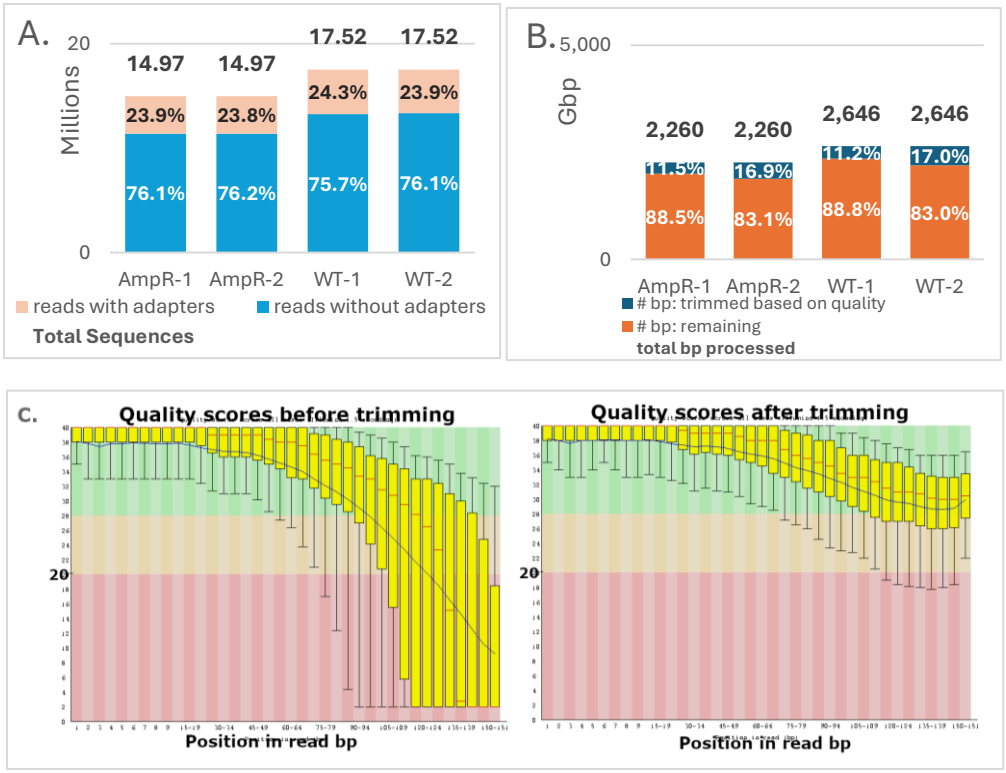

Figure 2. Changes after trimming in the sample sequences. The reads were processed with Trim-Galore!, while their quality was checked before and afterwards with FastQC. **A)** Reads contaminated with adapters. Even though more reads were collected for the WT sample, a similar proportion of around 24% of them was detected to have adaptors. **B)** Filtering base pairs based on quality. Due to a higher number of reads, a higher number of base pairs was processed for the WT. Around 11% of the forward read base pairs from the 3' end failed the quality threshold of Phred score of 20,

whereas that proportion was higher for the reverse pairs – around 17%. **C) Quality per base graph of AmpB-resistant reverse reads before and after trimming.** The per base quality significantly improved after trimming, with all values within the good quality range (>28, green), and the 10% and 90% falling in the reasonable quality range (orange, >20). However, the fall of quality at the end of sequencing is expected as the chemicals used for the process start degrading with time. Alternatively, it might result from the error eg bubbles in the sample, as some tiles showed low quality in the scan.

Genomic coverage and ploidy

Median coverage depth was equal to 113 for ampB-resistant and 125 for WT sample. Ploidy estimation pointed to differences in the chromosome copy number between ampB-resistant and WT cells – the drug-resistant cell line showed a lack of one copy of chromosome 6 and an extra copy in chromosomes 19, 22 and 27 (***Figure 3***).

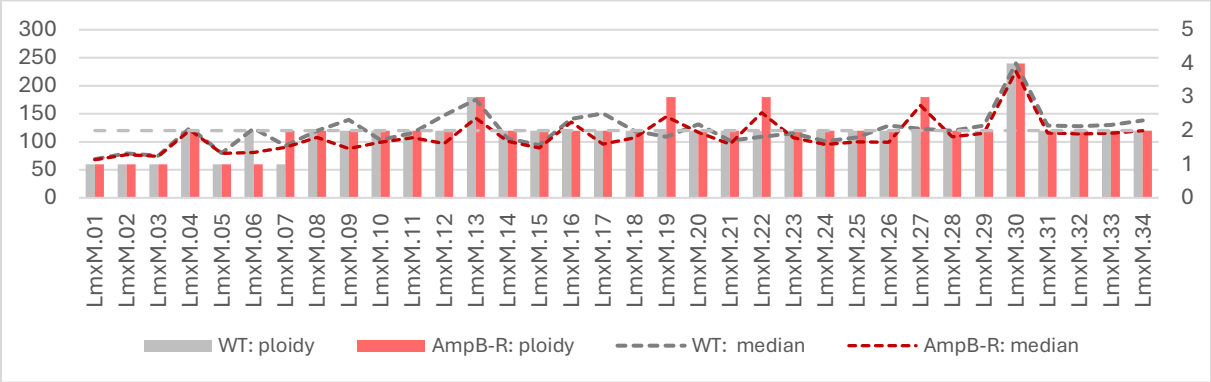

Figure 3. Ploidy estimation for ampB-resistant (ampB-R) and WT samples. The ampB-R *Leishmania mexicana* had gained an extra copy of chromosomes 19, 22 and 27, and a lack of chromosome 6. The ploidy estimation was based on the proportion of chromosome's median length to the whole genome median. The invalid estimation of a single copy in chromosomes 1-3 and 5-7 is due to the lack of correction for the chromosome length.

SNP detection

A total of 54 SNPs fulfilling the filtering criteria was detected for the drug-resistant sample (***Table 2***), whereas 36 were unique for the WT. 5270 SNPs were shared by both cell lines.

Disproportionally bigger share of SNPs unique to the AmpB-resistant cells were located on chromosomes 3 and 15 when compared to other sets (13% and 22% for AmpB-R vs 1.2% and 1.4% in both and none in the WT, respectively for 3 and 15 chromosome). 11% were located in not-annotated part of the reference genome. Functionally, 49 were missense variants, whereas 5 resulted in a gained STOP codon. Many of the affected proteins form membranes or participate in energy metabolism. Importantly, lanosterol 14-alpha demethylase is a key enzyme in sterol biosynthesis pathway.

Table 2. SNPs unique for the AmpB-resistant *Leishmania mexicana*. A total of 54 SNPs were unique for that sample group. Notably, one of the affected genes was responsible for the production of lanosterol 14-demethylase responsible for sterol biosynthesis. Many of other affected proteins are membrane components, are responsible for cell motility or energy metabolism. Chromosomes 3 and 15 are especially rich in unique SNPs.

Chromosome	ID	Position	REF (ref.)	ALT (alt.)	Nucleotide change	Amino acid change	Mutation type	Impact	Genotype*	Affected protein	Inferred function
unassembled contigs	LmxM.33.1590	91966	T	C	c.134T>C	p.Val45Ala	missense	MODERATE	1/1	tuzin-like protein	membrane component
	LmxM.33.1900	211757	G	T	c.430G>T	p.Val144Leu	missense	MODERATE	0/1	hypothetical protein	membrane component
	LmxM.30.0450d	270471	T	G	c.46A>C	p.Ile16Leu	missense	MODERATE	0/1	hypothetical protein	membrane component
	LmxM.30.0450e	304775	G	T	c.523C>A	p.Gln175Lys	missense	MODERATE	1/1	hypothetical protein	membrane component
		304787	T	G	c.511A>C	p.Met171Leu	missense	MODERATE	1/1		
	LmxM.34.0520a	384326	T	C	c.77T>C	p.Leu26Pro	missense	MODERATE	1/1	hypothetical protein	unknown
LmxM.02	LmxM.02.0310	122038	C	G	c.1535G>C	p.Arg512Pro	missense	MODERATE	0/1	paraflagellar rod component, putative	cell motility
	LmxM.02.0580	242695	G	T	c.1779G>T	p.Glu593Asp	missense	MODERATE	0/1	hypothetical protein, conserved	unknown
LmxM.03	LmxM.03.0270	67844	C	G	c.726C>G	p.Asp242Glu	missense	MODERATE	1/1	FYVE zinc finger/Apolipoprotein A1/A4/E domain containing protein, putative	lipid pathways, metal ion binding
		70050	G	C	c.2932G>C	p.Val978Leu	missense	MODERATE	0/1		
	LmxM.03.0350	97488	C	T	c.1381C>T	p.Pro461Ser	missense	MODERATE	0/1	hypothetical protein	energy metabolism
	LmxM.03.0360	106289	C	T	c.3029C>T	p.Ala1010Val	missense	MODERATE	0/1	hypothetical protein	unknown
	LmxM.03.0490	165044	G	A	c.298G>A	p.Gly100Ser	missense	MODERATE	0/1	hypothetical protein, conserved	membrane component
	LmxM.03.0510	179643	T	A	c.6395T>A	p.Val2132Glu	missense	MODERATE	0/1	hypothetical protein, conserved	post-translational modification
	LmxM.03.0530	191350	G	A	c.5320G>A	p.Asp1774Asn	missense	MODERATE	0/1	hypothetical protein, conserved	post-transcription modification
LmxM.04	LmxM.04.1140	392587	TGTGTGAC	TGTGTGTC	c.29T>A	p.Val10Asp	missense	MODERATE	./1	hypothetical protein	unknown
LmxM.08	LmxM.08_29.2020	315538	C	G	c.1011C>G	p.Tyr337*	stop_gained	HIGH	0/1	5'-AMP-activated protein kinase catalytic subunit alpha, putative	energy metabolism
	LmxM.08.0720	1451503	A	G	c.139A>G	p.Asn47Asp	missense	MODERATE	1/1	amastin-like protein, putative	membrane component
LmxM.09	LmxM.09.1400	505746	G	C	c.1013C>G	p.Ala338Gly	missense	MODERATE	0/1	hypothetical protein, unknown function	carbohydrate metabolism, ion binding, membrane component
LmxM.11	LmxM.11.1100	443299	A	T	c.527A>T	p.Asn176Ile	missense	MODERATE	1/1	Lanosterol 14-alpha demethylase	sterol metabolism, metal ion binding, membrane biogenesis
	LmxM.11.1220	474875	G	T	c.859G>T	p.Ala287Ser	missense	MODERATE	1/1	ATP-binding cassette protein subfamily A, member 2, putative	transmembrane transport, membrane component, ATP binding and hydrolysis
		478611	C	T	c.4595C>T	p.Pro1532Leu	missense	MODERATE	1/1		
LmxM.15	LmxM.15.0290	114538	G	A	c.221G>A	p.Gly74Asp	missense	MODERATE	0/1	hypothetical protein, conserved	unknown
		116409	G	A	c.2092G>A	p.Glu698Lys	missense	MODERATE	0/1		
	LmxM.15.0440	161461	C	T	c.295C>T	p.Pro99Ser	missense	MODERATE	0/1	tb-292 membrane associated protein-like protein	protein degradation
		161648	C	T	c.482C>T	p.Pro161Leu	missense	MODERATE	0/1		
		161693	A	C	c.527A>C	p.Asp176Ala	missense	MODERATE	0/1		
	LmxM.15.0490	175382	C	A	c.746C>A	p.Pro249Gln	missense	MODERATE	0/1	hypothetical protein, conserved	unknown
		175411	G	A	c.775G>A	p.Ala259Thr	missense	MODERATE	0/1		
	LmxM.15.0500	178486	T	C	c.808T>C	p.Cys270Arg	missense	MODERATE	0/1	serine peptidase, Clan SJ, family S16, putative, Fidgetin, putative, katanin-like protein	energy metabolism
		178672	A	G	c.994A>G	p.Thr332Ala	missense	MODERATE	0/1		
	LmxM.15.0510	181173	A	G	c.28A>G	p.Ser10Gly	missense	MODERATE	0/1	ecotin, putative	inhibitor of serine proteases
	LmxM.15.0530	189246	A	G	c.2512A>G	p.Asn838Asp	missense	MODERATE	0/1	hypothetical protein, conserved	membrane component
	LmxM.15.0630	236457	G	T	c.1564G>T	p.Ala522Ser	missense	MODERATE	0/1	hypothetical protein, unknown function	unknown
LmxM.16	LmxM.16.0760	263886	C	T	c.28G>A	p.Glu10Lys	missense	MODERATE	0/1	transaldolase, putative	energy metabolism, molecular function
LmxM.17	LmxM.17.1440	650650	T	C	c.479T>C	p.Val160Ala	missense	MODERATE	0/1	ion transport protein, putative	membrane component, ion transport
LmxM.20	LmxM.36.2600	1036228	G	A	c.1768C>T	p.Gln590*	gained STOP	HIGH	1/1	cyclin-e binding protein 1-like protein	motility
	LmxM.36.6510	2477763	C	T	c.91G>A	p.Asp31Asn	missense	MODERATE	0/1	cop9 signalosome complex subunit, putative	ubiquitylation signalling
	LmxM.20.1120	3115467	A	G	c.9668A>G	p.Asp3223Gly	missense	MODERATE	0/1	phosphatidylinositol 3-kinase, putative	cell proliferation, energy metabolism
	LmxM.20.1500	3271199	G	A	c.982C>T	p.Gln328*	gained STOP	HIGH	0/1	hypothetical protein, conserved	nucleus component
LmxM.21	LmxM.21.0430	130360	TGCAGCAGCAGCAGCAG	AGCAGCAGCAGCAGCAG	c.575T>A	p.Leu192Gln	missense	MODERATE	./1	hypothetical protein, conserved	posttranscriptional regulation of gene expression
LmxM.22	LmxM.22.1650	668718	C	A	c.660C>A	p.Tyr220*	gained STOP	HIGH	0/1	CobW/HypB/UreG, nucleotide-binding domain containing protein, putative	cobalamin biosynthesis
LmxM.24	LmxM.24.0100	19035	C	T	c.367C>T	p.Pro123Ser	missense	MODERATE	0/1	Calmodulin-binding, putative	motility
	LmxM.24.0690	247059	G	A	c.320G>A	p.Trp107*	gained STOP	HIGH	0/1	hypothetical predicted transmembrane protein	membrane component
LmxM.26	LmxM.26.0710	184583	A	T	c.2240T>A	p.Leu747His	missense	MODERATE	0/1	Sphingosine kinase	energy metabolism
LmxM.27	LmxM.27.0680	257164	A	G	c.212A>G	p.Lys71Arg	missense	MODERATE	0/1	amino acid permease, putative	membrane component
LmxM.28	LmxM.28.3030	1129692	C	T	c.2684G>A	p.Arg895Lys	missense	MODERATE	1/1	Nucleoporin NUP149	mRNA export from nucleus
		1130052	C	T	c.2324G>A	p.Arg775Lys	missense	MODERATE	1/1		
LmxM.29	LmxM.29.1080	352626	A	G	c.5585A>G	p.Gln1862Arg	missense	MODERATE	0/1	hypothetical protein, unknown function	protein interaction
LmxM.31	LmxM.31.1910	737974	A	C	c.1508T>G	p.Leu503Arg	missense	MODERATE	1/1	hypothetical protein, conserved	unknown
LmxM.32	LmxM.32.1160	430042	G	T	c.268G>T	p.Ala90Ser	missense	MODERATE	0/1	hypothetical protein, conserved	membrane component
	LmxM.32.3210	1387300	A	T	c.494A>T	p.Asp165Val	missense	MODERATE	0/1	beta prime cop protein, putative	protein transport
	LmxM.32.3220	1394239	C	A	c.1162C>A	p.Gln388Lys	missense	MODERATE	0/1	hypothetical protein, conserved	ion binding, post-translational processing
LmxM.33	LmxM.33.4060	1535372	G	C	c.1156G>C	p.Ala386Pro	missense	MODERATE	0/1	ubiquitin hydrolase, putative	deubiquitination

Proteomics: the impact of the lanosterol 14-alpha mutation

CYP51 protein characteristics

The similarity between chain A of CYP51 of *L. infantum* (Genbank: GenBank: ABM89546.1) and 3L4D *L. infantum*, as bound to fluconazole, showed a 97.5% and 96.7% similarity against the *L. mexicana* CYP51 (GenBank: ACU00618.1; Supplementary figure 1), respectively. The protein structures were superimposed with each other, showing a high visual overlap (***Figure 4***; RSMD <1 Å). 68 atoms were rejected during alignment as their RSMD exceeded 1 Å.

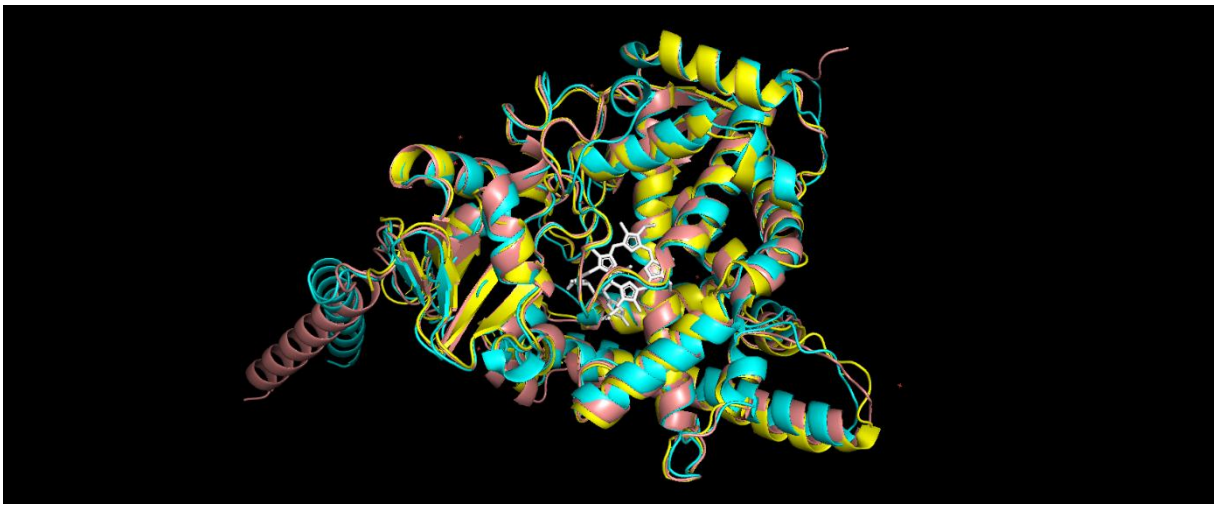

Figure 4. Superimposed protein structures of chain A of CYP51 of *L. mexicana* WT (predicted by Alphafold), N176I mutant (predicted by D-I-TASSER) and *L. infantum* 3L4D (complex with fluconazole). Both proteins show very high similarity against the *L.mex* WT (RSMD=0.953 Å for the mutant, 0.613 Å for the *L.infantum*), with D-I-TASSER prediction of the mutant diverging at the 5' end tail of the protein. This might be due to different software used for the predictions as the mutation is far from this location. Aligning of the molecules was performed in PyMOL.

CYP51 forms a complex of 4 chains (***Figure 5A***), with each binding the substrate in the active site in high proximity to the heme iron (***Figure 5B***, yellow), as described by Hargrove (2011). Interestingly, the mutation N176I described previously (Mwenechanya, 2017) is located approximately 13.3 Å from the active site (***Figure 5C***)

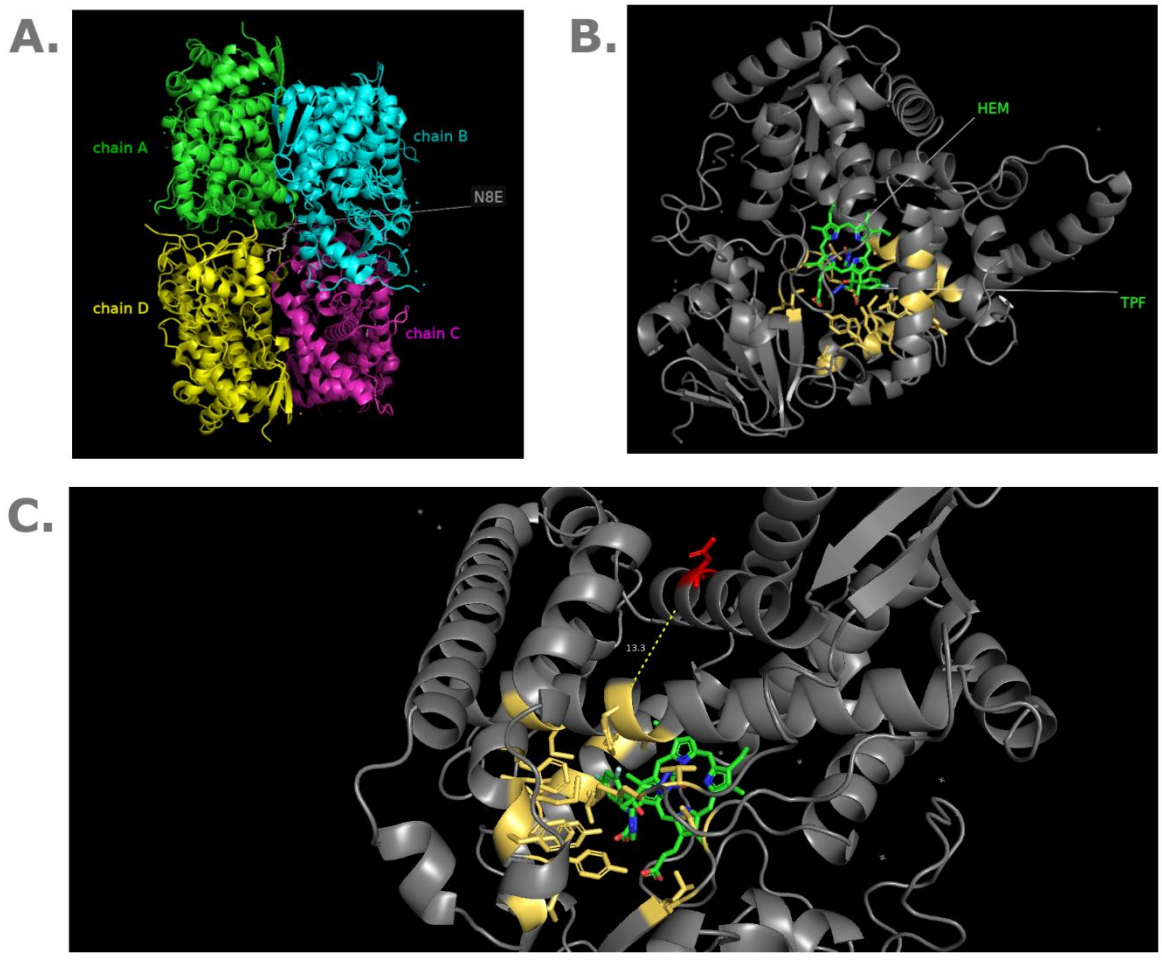

Figure 5. The visualisation of the protein structure of CYP51 of *Leishmania infantum*. CYP51 forms complexes of 4 chains **(A)**, with each binding its substrate in the active pocket **(B, yellow)** in high proximity to the heme iron molecule in its centre. The N176I mutation **(C, red)** that might underlie the ampB resistance is, however, located approximately 13.3 Å from the binding pocket.

Ligand docking

Optimal ligands positions docked to the WT and N176I proteins were different from each other (Figure 6). Still, they shared an oblong shape, suitable for small pores in the dense CYP51 structure. The most optimal positions for CYP51 had the Gibbs free energy (ΔG) of -8.6841 and -8.4867 for WT and a mutant, respectively.

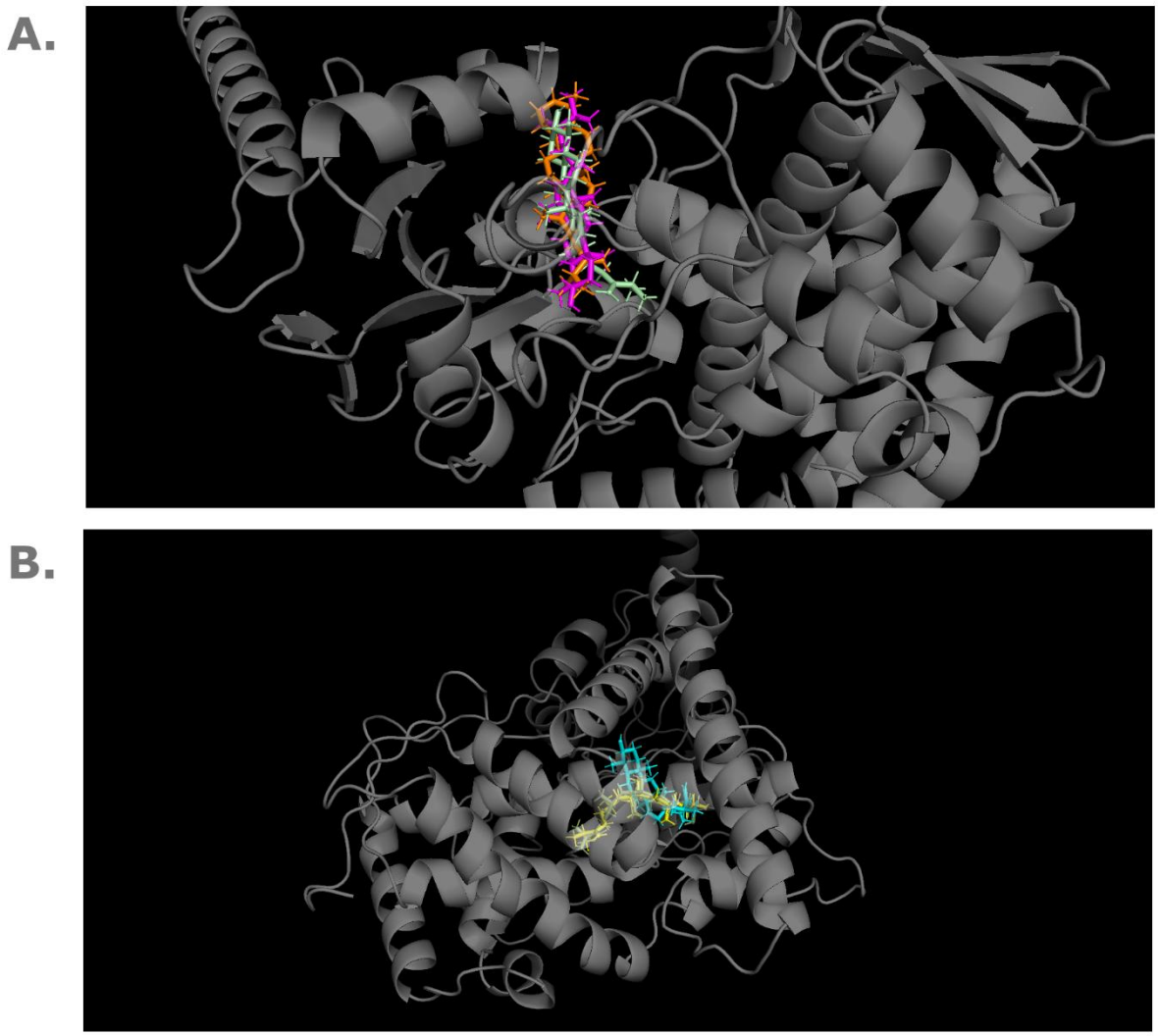

Figure 6. Top docking positions of obtusifoliol with a WT (A) and mutant (B) CYP51. Obsifoliol binds at the active site, though assumes different positions. The top 3 poses for the WT share a notably oblong shape and the presence at the active site. For each model, the top alignments are very similar, with the best one shown in magenta for WT (ΔG=-8.6841) and olive green for the mutant (ΔG=-8.4867). The discrepancies between WT and mutant docking can be due to an imprecise active site marking in Swissdock, that might not align exactly between models.

Molecular dynamics simulation

The molecular dynamics simulation did not show any notable differences for the WT and mutant in terms of their potential energy and temperature-reaction. Binding of the ligand seemed to decrease the fluctuations in gyrus of radius for both models (**Figure 7**). Moreover, the change seemed bigger for mutant, as it showed more fluctuations in shape without the ligand, stabilising upon binding.

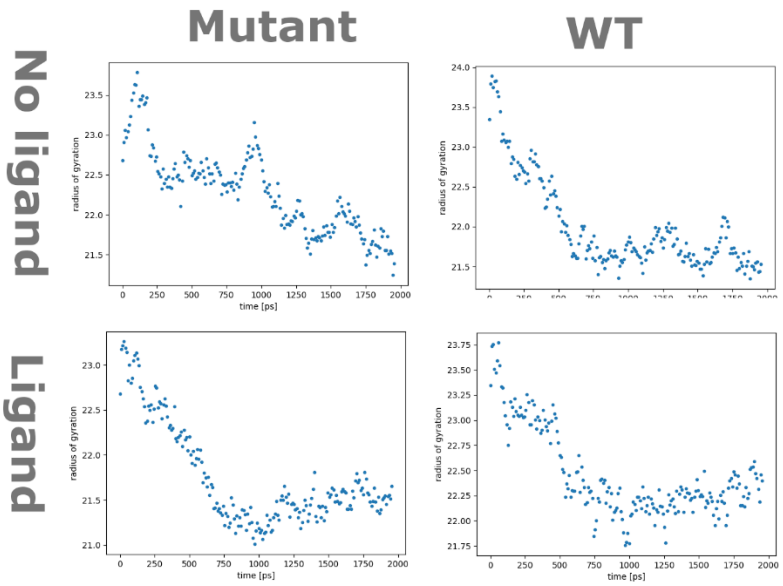

Figure 7. Changes in radius of gyration in time for WT and N176I CYP51 mutant in *Leishmania mexicana* models generated in UNRES-MD. Mutant CYP51 showed more fluctuations in shape in time than the WT, therefore stabilising more in the presence of the ligand.

Intracellular localisation

Even though *L. mexicana* CYP51 had no signal sequence detected with SignalP, Deeploc predicted it to localise to the peripheral membrane (probability=0.8010) endoplasmic reticulum (probability = 0.8754) for both the WT and the mutant.

Metabolomics analysis

Explorative results

Overall, many peak intensities were different between sample groups of WT and AmpB-resistant cells (**Figure 8A**). With significance threshold of log fold change of 2 and a p value of 0.05, 226 peaks were downregulated in intensity and 82 were upregulated in the drug resistant strain (**Figure 8B**).

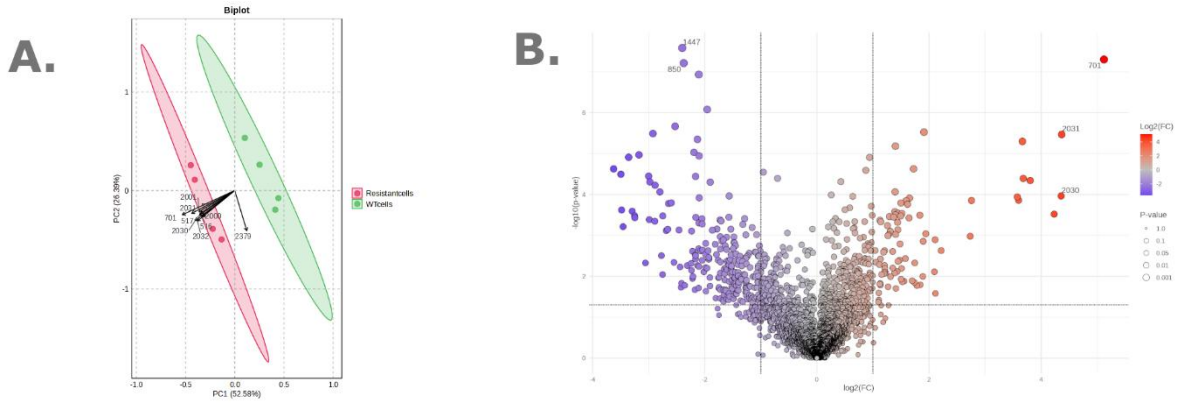

Figure 8. Differential peak intensity in mass spectrometry of WT and AmpB-resistant *Leishmania mexicana*. The dimensional reduction of variance in PCA biplot **(A)** shows a divergent profiles of both groups, with a main component responsible for more than half of variance. The fuelling variables peak IDs are noted as vectors. This result is corroborated by the volcano plot of all log-transformed peak intensities **(B)**. A total of 308 peaks showed a log fold change above 2 and statistical significance (threshold showed as a dashed line), with the top 10 differential intensities annotated.

Changes in sterol biosynthesis pathway

The highest fold change was observed for peak 701 **(Figure 9)**, upregulated by log fold change 5.12. It cannot be identified with full confidence; however, it could correspond to dehydrated 4,4-Dimethyl-5alpha-cholesta-8,14,24-trien-3beta-ol, identified in this conditions previously (Mwenechanya, 2011). Similarly decreased were peaks 1242 (logFC = 3.20; **Figure 9**), 2092 (logFC = 2.63; **Figure 9**) and 2093 (logFC = 1.52; **Figure 9**), which were likely related to sterols. However, those peaks did not meet the strict filtering criteria. Contrary change was noticed for peak 655, identified as ergosterol (log FC = -3.36; **Figure 9**). In the context of the sterol biosynthesis, the cholestane-like and demethylated sterols - intermediate or bypass products - are upregulated in mutant, while ergosterol – end product – is downregulated.

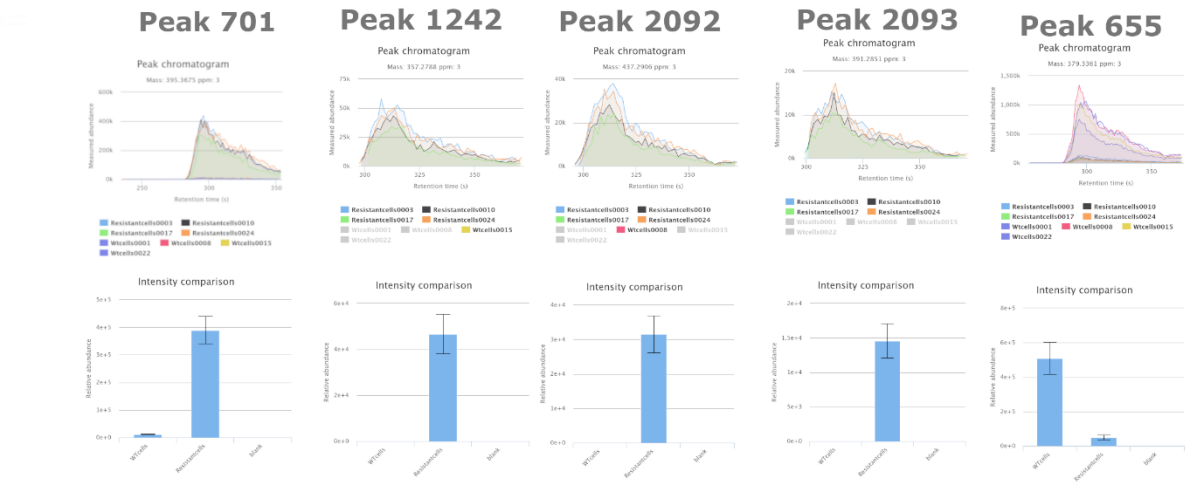

Figure 9. Changes in peaks related to sterol biosynthesis. Peaks 701, 1242, 2092 and 2093 were downregulated; however peaks 1242 (logFC=3.20), 2092 (logFC=2.63) and 2093 (logFC=1.52) did not pass strict statistical filtering in Metaboanalyst. Highly upregulated peak 701 (logFC=5.12) has been identified as a dehydrated 4,4-Dimethyl-5alpha-cholesta-8,14,24-trien-3beta-ol, whereas accompanying peaks are likely related to sterols and can't be identified specifically. Downregulated peak 655 likely corresponds to ergosterol (log FC = -3.36).

Changes in oxidative stress response

L-Arginine and L-Proline, sourced extracellularly in *Leishmania*, were both downregulated in the drug-resistant sample (logFC=-1.65 and logFC=-1.41, respectively), which might indicate cells' increased need for response to reactive oxygen species, energy or osmolytic buffering.

Changes can also be noted in the glycolytic pathway; however, sugars often show cross-detection in mass spectrometry and those results are of lower confidence. The end product, pyruvate is upregulated in mutant (log FC=0.37), while the level glyceraldehyde (logFC = -0.42) and some pentose sugars is likely lower. Notably, the molecules responsible for oxidative stress response might be downregulated – carnosine (logFC = -0.75), creatine (logFC = -0.57), cysteines (logFC= -1.25) and ornithine (logFC = -2.86).

Discussion

Overall, this report corroborates previous findings on the role of sterols in AmpB resistance in *Leishmania mexicana* with bioinformatics tools and polyomic approach. An integrated data from metabolomics data, proteomic structure simulation and genomic analysis points to the decreased levels of ergosterol caused by the point mutation in 14-alpha demethylase.

Furthermore, metabolomics and genomics data point to some changes in the response of mutant cell line to oxidative stress. Some SNPs unique for the mutant cell lines are involved in energy metabolism. Also, is corroborated by the targeted mass spectrometry or fragmentation studies, the amount of metabolites responsible for the response to ROS is higher in the mutant.

This report consisted only of the subset of data used in other studies (Hargrove, 2011; Mwenechanya, 2017). Therefore, its biggest limitations is a small, homogenous sample size. Each group consists of only one population of cells, cultured in parallel from the same source. A homogenous population of Leishmania potentially accounts only for a subset of naturally occurring AmpB-resistant organisms. Moreover, it's parallel growth does not show the variance in genome caused by environmental factors or differential age. However, the conclusions regarding the sterol pathway's involvement and the membrane fluidity is shared with other studies on Leishmania from patients non-responsive to AmpB, likely more heterogenous (Purkait, 2012). It is also important to remember that the mechanism of AmpB resistance described here is not an exhaustive account of all possible mechanisms that might exist in parallel.

Changes in nucleosides and amino acids, as well as in the membrane permeability also observed for pentamidine resistance (Basselin et al, 1997; Basselin et al, 1998). Interestingly, the AmpB resistant cell line showed no cross resistance for pentamidine and azoles, drugs thought to be working via the sterol pathway (pentamidine: Mukherjee et al, 2020, azoles: White, 1997; Sanglard 1998). That might be explained by multi-modal drug action, such as a theocratised CYP5122A1 relevance in anti-leishmania action of azoles (Jin et al, 2023). Therefore, it stands to reason that AmpB resistance is not limited to the absence of ergosterol, but supported by other adaptations within the cell line. Still, a return of AmpB sensitive after re-introduction of ergosterol suggests its leading role in the resistance in this cell line. Hence, another possible hypothesis is the existence of the ergosome, that acts together to facilitate the sterol biosynthesis and is more resistant to the rise of resistance through partial redundance in the action of participating enzymes. The evidence for such complex might be found within the unique SNPs for the drug resistant strain that were not matched with an annotated genome of the reference species. The reference genome has not been uncovered in its entirety, and further investigations might uncover features unique for this species or genus.

The study also provides more input on how the CYP51 N176I mutation interferes with it's processing of substrates. The simulation with DeepLoc and SignalP negate the hypothesis of a differential cell localisation. Although the mutation is not in the active site, another hypothesis suggest altered ligand

binding. Docking simulations from SwissDock for each model result in similar ligand docking, oblong, likely in order to reach the active site in the centre of the structure. Moreover, UNRES shows a decreased fluctuations of protein structure in space after binding the ligand, which might correlate with keeping the ligand enclosed at the active site. The rigidity of the protein seems affected in the mutant, fluctuating more when compared to the wild-type.

To sum up, this report corroborates previous findings. Together, it provides invaluable insight into AmpB resistance in *Leishmania mexicana*. Knowing how the parasite evades new treatment will help develop a new class of drugs in time to replace AmpB as the main treatment if resistance arises in the wider population. Nonetheless, more studies should follow to corroborate this result. Primarily, it should be replicated in Leishmania mexicana grown for a different time and from different source samples. The possibility of targeting the weakened oxidative stress response of the drug-resistant strain should also be investigated as it might lead to the development of combined or alternative treatments.

References

Anderson, T.M. *et al.* (2014) "Amphotericin forms an extramembranous and fungicidal sterol sponge," *Nature Chemical Biology 2014 10:5*, 10(5), pp. 400–406. Available at: https://doi.org/10.1038/nchembio.1496.

Basselin, M., Lawrence, F. and Robert-Gero, M. (1997) "Altered transport properties of pentamidine-resistant Leishmania donovani and L. amazonensis promastigotes," *Parasitol Res*, (83), pp. 413–418.

Beneke, T. *et al.* (2023) "Genome sequence of Leishmania mexicana MNYC/BZ/62/M379 expressing Cas9 and T7 RNA polymerase," *Wellcome Open Research*, 7, p. 294. Available at: https://doi.org/10.12688/WELLCOMEOPENRES.18575.2.

Brown, N.P., Leroy, C. and Sander, C. (1998) "MView: a web-compatible database search or multiple alignment viewer.," Bioinformatics, 14(4), pp. 380–381. Available at: https://doi.org/10.1093/BIOINFORMATICS/14.4.380.

Bugnon, M. et al. (2024) "SwissDock 2024: major enhancements for small-molecule docking with Attracting Cavities and AutoDock Vina," Nucleic Acids Research, 52(W1), pp. W324–W332. Available at: https://doi.org/10.1093/NAR/GKAE300.

Gaffi (2018) *Gilead reduces price of AmBisome (liposomal amphotericin B) for cryptococcal meningitis in HIV/AIDS*. Available at: https://gaffi.org/gilead-reduces-price-of-ambisome-liposomal-amphotericin-b-for-cryptococcal-meningitis-in-hiv-aids/ (Accessed: May 12, 2025).

Gloaguen, Y. et al. (2017) "PiMP my metabolome: an integrated, web-based tool for LC-MS metabolomics data," Bioinformatics, 33(24), p. 4007. Available at: https://doi.org/10.1093/BIOINFORMATICS/BTX499.

Graf, F.E. *et al.* (2013) "Aquaporin 2 Mutations in Trypanosoma brucei gambiense Field Isolates Correlate with Decreased Susceptibility to Pentamidine and Melarsoprol," *PLOS Neglected Tropical Diseases*, 7(10), p. e2475. Available at: https://doi.org/10.1371/JOURNAL.PNTD.0002475.

Hargrove, T.Y. *et al.* (2011) "Substrate preferences and catalytic parameters determined by structural characteristics of sterol 14α-demethylase (CYP51) from Leishmania infantum," *Journal of Biological Chemistry*, 286(30), pp. 26838–26848. Available at: https://doi.org/10.1074/jbc.M111.237099.

Jin, Y. *et al.* (2023) "CYP5122A1 encodes an essential sterol C4-methyl oxidase in Leishmania donovani and determines the antileishmanial activity of antifungal azoles," *Research Square*, p. rs.3.rs-3185204. Available at: https://doi.org/10.21203/RS.3.RS-3185204/V1.

Jumper, J. *et al.* (2021) "Highly accurate protein structure prediction with AlphaFold," *Nature 2021 596:7873*, 596(7873), pp. 583–589. Available at: https://doi.org/10.1038/s41586-021-03819-2.

Kumari, S. *et al.* (2022) "Amphotericin B: A drug of choice for Visceral Leishmaniasis," *Acta Tropica*, 235, p. 106661. Available at: https://doi.org/10.1016/J.ACTATROPICA.2022.106661.

Lepesheva, G.I. and Waterman, M.R. (2006) "Sterol 14α-Demethylase Cytochrome P450 (CYP51), a P450 in all Biological Kingdoms," *Biochimica et biophysica acta*, 1770(3), p. 467. Available at: https://doi.org/10.1016/J.BBAGEN.2006.07.018.

Mesa-Arango, A.C., Scorzoni, L. and Zaragoza, O. (2012) "It only takes one to do many jobs: Amphotericin B as antifungal and immunomodulatory drug," *Frontiers in Microbiology*, 3(AUG), p. 29276. Available at: https://doi.org/10.3389/FMICB.2012.00286/BIBTEX.

Mukherjee, S. *et al.* (2020) "Sterol 14-α-demethylase is vital for mitochondrial functions and stress tolerance in Leishmania major," *PLOS Pathogens*, 16(8), p. e1008810. Available at: https://doi.org/10.1371/JOURNAL.PPAT.1008810.

Mwenechanya, R. *et al.* (2017) "Sterol 14α-demethylase mutation leads to amphotericin B resistance in Leishmania mexicana," *PLoS Neglected Tropical Diseases*, 11(6). Available at: https://doi.org/10.1371/journal.pntd.0005649.

Ødum, M.T. et al. (2024) "DeepLoc 2.1: multi-label membrane protein type prediction using protein language models," Nucleic Acids Research, 52(W1), pp. W215–W220. Available at: https://doi.org/10.1093/NAR/GKAE237.

Pang, Z. *et al.* (2024) "MetaboAnalyst 6.0: towards a unified platform for metabolomics data processing, analysis and interpretation," *Nucleic Acids Research*, 52(W1), pp. W398–W406. Available at: https://doi.org/10.1093/NAR/GKAE253.

Peacock, C.S. *et al.* (2007) "Comparative genomic analysis of three Leishmania species that cause diverse human disease," *Nature genetics*, 39(7), p. 839. Available at: https://doi.org/10.1038/NG2053.

Pettersen, E.F. *et al.* (2004) "UCSF Chimera—A visualization system for exploratory research and analysis," *Journal of Computational Chemistry*, 25(13), pp. 1605–1612. Available at: https://doi.org/10.1002/JCC.20084.

Pountain AW, Barrett MP. Untargeted metabolomics to understand the basis of phenotypic differences in amphotericin B-resistant *Leishmania* parasites. Wellcome Open Res. 2019 Nov 13;4:176. doi: 10.12688/wellcomeopenres.15452.1. PMID: 32133420; PMCID: PMC7041363.

Purkait, B. *et al.* (2012) "Mechanism of amphotericin B resistance in clinical isolates of Leishmania donovani," *Antimicrobial Agents and Chemotherapy*, 56(2), pp. 1031–1041.

Robinson, J.T. et al. (2017) "Variant review with the integrative genomics viewer," Cancer Research, 77(21), pp. e31–e34. Available at: https://doi.org/10.1158/0008-5472.CAN-17-0337/SUPPLEMENTARY-VIDEO-S1.

Röhrig, U.F. et al. (2023) "Attracting Cavities 2.0: Improving the Flexibility and Robustness for Small-Molecule Docking," Journal of Chemical Information and Modeling, 63(12), pp. 3925–3940. Available at: https://doi.org/10.1021/ACS.JCIM.3C00054/ASSET/IMAGES/LARGE/CI3C00054_0009.JPEG.

Sanglard, D. *et al.* (1998) "Amino Acid Substitutions in the Cytochrome P-450 Lanosterol 14α-Demethylase (CYP51A1) from Azole-Resistant Candida albicans Clinical Isolates Contribute to Resistance to Azole Antifungal Agents," *Antimicrobial Agents and Chemotherapy*, 42(2), p. 241. Available at: https://doi.org/10.1128/AAC.42.2.241.

Singh, A.K., Papadopoulou, B. and Ouellette, M. (2001) "Gene Amplification in Amphotericin B-Resistant Leishmania tarentolae," *Experimental Parasitology*, 99(3), pp. 141–147. Available at: https://doi.org/10.1006/EXPR.2001.4663.

Ślusarz, R. *et al.* (2025) "UNRES web server: Extensions to nucleic acids, prediction of peptide aggregation, and new types of restrained calculations," *Journal of Molecular Biology*, p. 168968. Available at: https://doi.org/10.1016/J.JMB.2025.168968.

Srivastava, P. et al. (2011) "Unusual Case of Resistance to Amphotericin B in Visceral Leishmaniasis in a Region in India Where Leishmaniasis Is Not Endemic," Journal of Clinical Microbiology, 49(8), p. 3088. Available at: https://doi.org/10.1128/JCM.00173-11.

Teufel, F. *et al.* (2022) "SignalP 6.0 predicts all five types of signal peptides using protein language models," *Nature Biotechnology* 2022 40:7, 40(7), pp. 1023–1025. Available at: https://doi.org/10.1038/s41587-021-01156-3.

Uliana, S.R.B., Trinconi, C.T. and Coelho, A.C. (2018) "Chemotherapy of leishmaniasis: present challenges," *Parasitology*, 145(4), pp. 464–480. Available at: https://doi.org/10.1017/S0031182016002523.

White, T.C. (1997) "The Presence of an R467K Amino Acid Substitution and Loss of Allelic Variation Correlate with an Azole-Resistant Lanosterol 14 Demethylase in Candida albicans," 41(7), pp. 1488–1494.

WHO (2023) *Leishmaniasis*. Available at: https://www.who.int/news-room/fact-sheets/detail/leishmaniasis (Accessed: May 13, 2025).

Zhang, J. *et al.* (2019) "The fungal CYP51s: Their functions, structures, related drug resistance, and inhibitors," *Frontiers in Microbiology*, 10, p. 436065. Available at: https://doi.org/10.3389/FMICB.2019.00691/XML/NLM.

Zheng, W. *et al*, (2025) "Deep learning-based single- and multi-domain protein structure prediction with D-I-TASSER," *Nature Biotechnology*, in press (2025)

Supplementary figures

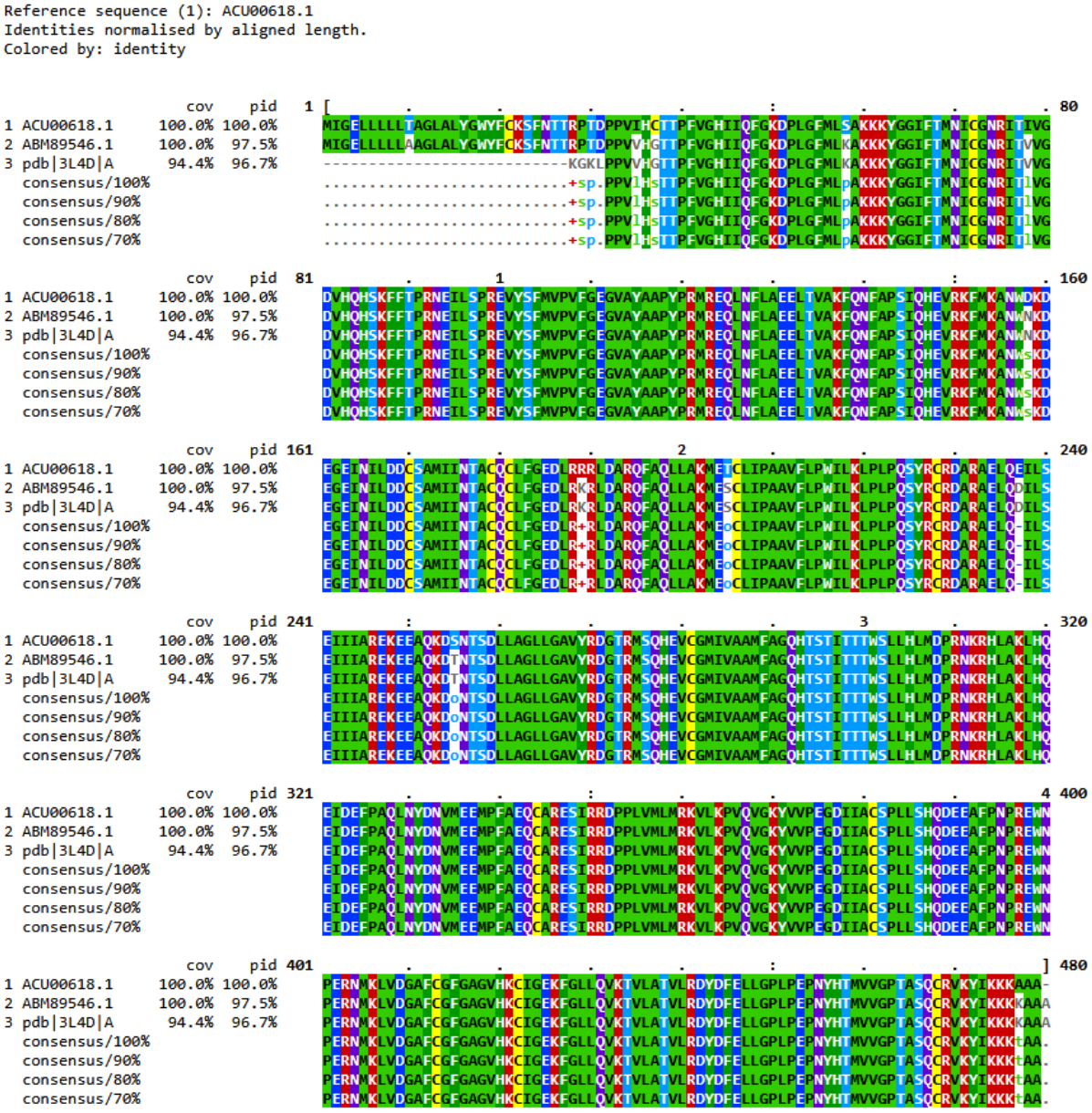

Supplementary figure 1. Sequence alignment from MView between CYP51 of *L. infantum* (NCBI Genbank: ABM89546.1), *L. mexicana* (NCBI Genbank: ACU00618) and chain A of L. infantum (pdb ID: 3L4D).

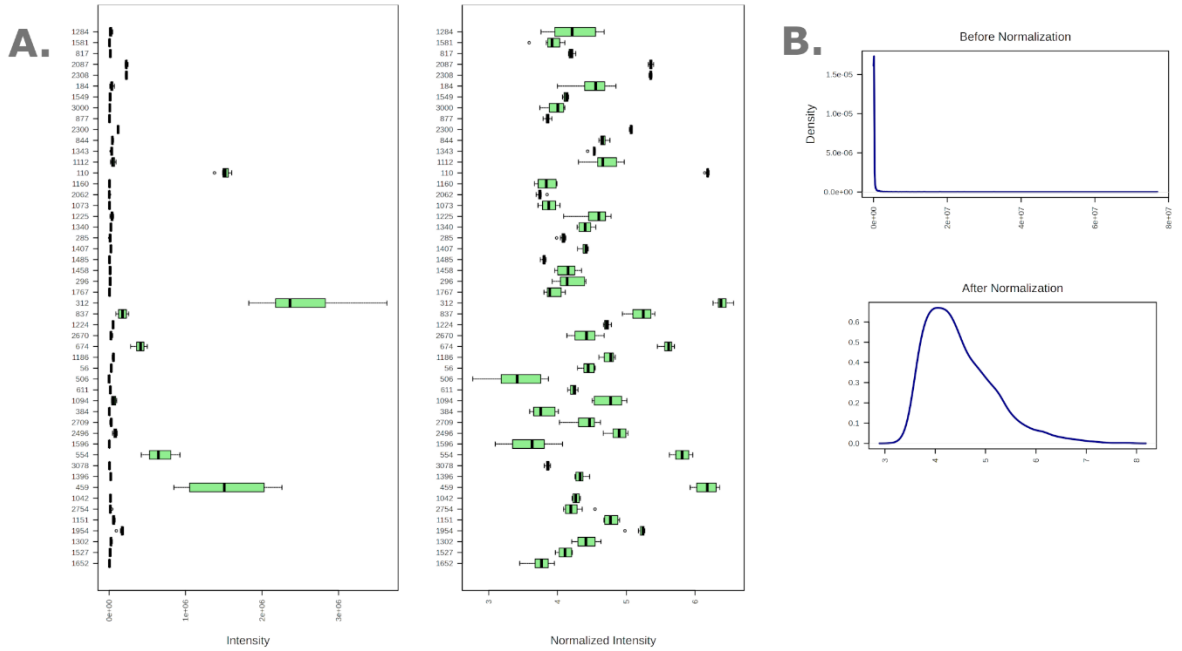

Supplementary figure 2. Log-transformation of the metabolomics results. During pre-processing, it was log-transformed to account for the high variability between the numerical scales for different metabolites. The result shows a normal distribution of data **(B)**. Furthermore, the transformation enables comparing the variable readings in one visualisation **(A)**. The readings were acquired with an Orbitrap Exactive Mass Spectrometer and a Sequant ZIC-HILIC column, and processed on MetaboAnalyst 6.0.